Boundary-Layer Meteorol (2014) 150:107–130
DOI 10.1007/s10546-013-9864-4

ARTICLE

Impacts of Mixing Processes in Nocturnal Atmospheric Boundary Layer on Urban Ozone Concentrations

Petra M. Klein · Xiao-Ming Hu · Ming Xue

Received: 14 December 2012 / Accepted: 12 August 2013 / Published online: 4 October 2013

Abstract A number of open questions remain regarding the role of low-level jets (LLJs) and nocturnal mixing processes in the buildup of tropospheric ozone. The prevalence of southerly winds and LLJs in the U.S. Southern Great Plains during summer makes this region an ideal site for investigating the structure of the nocturnal boundary layer and its impacts on urban air quality. Ozone (O_3) and nitrogen oxide concentrations measured at regulatory monitoring sites in the Oklahoma City (OKC) area and simulations with the Weather Research and Forecasting with Chemistry (WRF/Chem) model were analyzed to show how the nocturnal LLJ moderates boundary-layer mixing processes and air quality. Datasets collected during the Joint Urban 2003 campaign, which took place in July 2003 in OKC, provided detailed information about nocturnal boundary-layer structure and dynamics. In general, O_3 time series show the expected behavior that urban O_3 concentrations decrease at night due to nitrogen oxide titration reactions, but elevated O_3 concentrations and secondary O_3 peaks are also seen quite frequently after sunset. LLJs developed on most nights during the study period and were associated with strong vertical wind shear, which affected the boundary-layer stability and structure. Near-surface O_3 concentrations are higher during less stable nights when active mixing persists throughout the night. The WRF/Chem model results agree well with the observations and further demonstrate the role of LLJs in moderating nocturnal mixing processes and air quality. The highest nocturnal O_3 concentrations are linked to a strong LLJ that promotes both nocturnal long-range transport and persistent downward mixing of O_3 from the residual layer to the surface.

Keywords Low-level jet · Nocturnal boundary layer · Tropospheric ozone · Turbulent mixing · Urban air quality

P. M. Klein · M. Xue
School of Meteorology, University of Oklahoma, Norman, OK, USA

P. M. Klein (✉) · X.-M. Hu · M. Xue
Center for Analysis and Prediction of Storms, University of Oklahoma, Norman, OK, USA
e-mail: pkklein@ou.edu

1 Introduction

Photochemical pollutants, such as ground-level ozone (O_3), are known to peak primarily in summer during anticyclonic stagnation periods. During such episodes, ozone air-quality standards are often exceeded in and downwind of major urban areas. Although air pollution control strategies over the past decades have been widely successful, recent years have shown negligible or only slight improvements in air quality in many areas (EPA 2010). Thus, the current paradigm for O_3 formation, which focuses on the emission and accumulation of ozone precursors picking up during the morning urban rush hour followed by photochemical O_3 formation throughout the day, must be expanded. Hidy (2000) points out the sensitivity of O_3 concentrations to meteorological conditions and lists the vertical structure of wind speed and mixing processes as key factors. Athanassiadis et al. (2002) discussed uncertainties in estimating the daytime mixing height of the atmospheric boundary layer (ABL) from mesoscale model fields and its impact on O_3 predictions. They further concluded that downward mixing of O_3 trapped overnight in the residual layer in the early morning strongly influenced daytime O_3 peak concentrations. Brown et al. (2006) identified the stratification of the ABL at night as an important factor due to its impact on the dispersion of nitrogen oxide (NO_x) emissions. The stable surface layer that develops at night due to radiative cooling of the surface is frequently decoupled from the residual layer. The downward mixing of NO_x emissions from tall sources above the stable surface layer (e.g., from power plants) may be limited, while near-ground NO_x emissions in urban areas become trapped within the stable surface layer, where they react with O_3. Due to such titration reactions, very low O_3 concentrations are typically observed at urban surface monitoring sites. Velasco et al. (2008) measured O_3 and meteorological vertical profiles in the Mexico City basin and concluded that O_3 concentrations remained elevated within the residual layer above 200–500 m, while volatile organic compounds (VOCs) and NO_x emissions at night became trapped within a well-mixed urban surface layer that is decoupled form the residual layer. After sunrise, O_3 is mixed down to the ground, where it is initially reduced due to reactions with accumulated VOC and NO_x emissions, before O_3 production reactions start to dominate and trigger the increase in O_3 during the day. Based on O_3 soundings in Switzerland, Neu et al. (1994) concluded that more than 50 % of the daytime peak O_3 concentrations at the surface could be attributed to downward mixing of O_3 from the residual layer, i.e., that contributions from vertical mixing processes dominated over chemical production and advection in the daily O_3 buildup.

Recent studies with remote sensing instruments (Stutz et al. 2000, 2009) also clearly show pronounced vertical gradients of O_3 and NO_2 at night. In polluted and semipolluted areas, the causes of this inhomogeneous behavior are often surface emissions of NO, which then titrate O_3 close to the ground. At higher altitudes O_3 concentrations depend on the magnitude of vertical mixing and advection in the nocturnal boundary layer (NBL) but typically remain much higher throughout the night. During the morning transition of the NBL, air from different altitudes with different spatial and chemical histories is then mixed to provide the starting point for daytime O_3 formation. Simulations with a one-dimensional chemical transport model (Geyer and Stutz 2004a,b) further supported such experimental findings; it was confirmed that nocturnal chemistry strongly depends on altitude. In addition to NO emission rates, vertical mixing and its dependence on atmospheric stability were identified as key parameters, and the authors concluded that further studies were needed to quantify the influence of nocturnal mixing and chemistry on urban air quality.

Several studies have also shown that the chemistry and transport of polluted air at night by accelerated flow above the surface, a phenomenon manifest as the low-level jet (LLJ),

and related downward mixing of pollutants at night or during the next morning (Samson 1978; Banta et al. 1998; Zhang and Rao 1999; Solomon et al. 2000; Philbrick et al. 2003) play an important role. Such LLJs are a prominent feature of the NBL in the Southern Great Plains of the USA (Wexler 1961; Zhong et al. 1996; Whiteman et al. 1997; Higgins et al. 1997; Parish and Oolman 2010). Strong LLJs have been linked to enhanced nocturnal mixing and downward transport of turbulence from the level of the jet nose to the surface (Banta et al. 2003, 2006; Balsley et al. 2008), while the strongly stable, decoupled boundary layer is typical for weak LLJs (Banta et al. 2007). A more extensive summary of results related to the climatology, development, and impacts of LLJs in central Oklahoma can be found in Hu et al. (2013b).

Reitebuch et al. (2000) and Hu et al. (2013c) linked nocturnal mixing processes related to LLJ development or frontal passages to secondary, nocturnal O_3 peaks at surface monitoring sites. Secondary O_3 peaks in the evening and at night were also observed during ozone episodes in the OKC metropolitan area (Kastner-Klein et al. 2002). Simultaneous measurements of elevated O_3 concentrations at a rural site on a 620-m high mountain upwind of OKC, supported the hypothesis that downward mixing of O_3, transported aloft, triggered the elevated surface concentrations, but the lack of profile measurements of winds and O_3 prevented a more in-depth analysis of the role of nocturnal mixing. Eliasson et al. (2003) analyzed nocturnal surface O_3 concentrations observed in Gothenburg, Sweden, and identified both advection and vertical mixing as factors contributing to such events. They stressed that the frequent occurrences of such nocturnal maxima with concentrations reaching regulatory standards should be further investigated and taken into account as appropriate. Tong et al. (2011) conducted an extensive literature review and identified major gaps in the understanding of the formation of nocturnal O_3 maxima; they concluded that a consensus on the processes causing such nocturnal maxima is still lacking. Hu et al. (2013a) conducted sensitivity tests with a one-dimensional air chemistry transport model, and were able to show that enhanced nocturnal mixing in the presence of a LLJ produced nocturnal O_3 peaks observed at a site in the state of Maryland. Under such conditions, the residual layer and surface layer remain coupled, a situation described by Hu et al. (2013a) as a leaky residual layer.

In addition to the implications for urban air quality, NBL mixing processes are also known to affect the nocturnal horizontal temperature distribution (e.g., Fitzjarrald and Moore 1994; Acevedo and Fitzjarrald 2001). After sunset, during the early evening transition, turbulent kinetic energy and mixing have been found to rapidly decrease in the stable surface layer, which then often becomes decoupled from the residual layer aloft. Under such conditions, the temperature difference between a city and its rural environment, the urban heat island (UHI) intensity, is strongest at night and can be attributed to differences in the nocturnal urban and rural cooling rates, particularly during the early evening transition (Oke 1982). Hu et al. (2013b) investigated the role of mixing in the NBL in the formation of UHI events in the OKC metropolitan area during July 2003. They found that in the presence of strong LLJs, the NBL in rural terrain becomes deeper, more mixed, and less stable, leading to relatively small contrasts in urban and rural temperatures. During nights with relatively weak or absent LLJs, much larger temperature gradients and a much shallower, rural NBL are observed. Under such conditions, enhanced mixing and heat releases in the urban canopy layer have a strong influence on the temperature structure close to the surface, which causes larger contrasts between urban and rural temperature vertical profiles and, thus, a stronger UHI signature. An important finding was that NBL structure and mixing in rural areas, which was strongly correlated to the temperature gradient at rural Oklahoma Mesonet sites, was a good indicator of the UHI intensity.

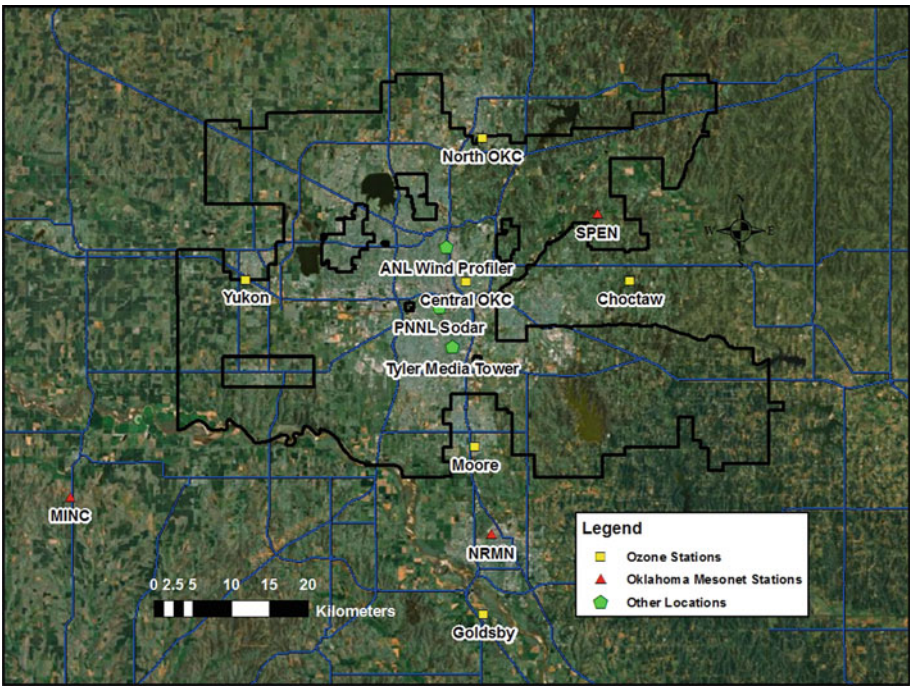

Fig. 1 Map of study area showing location of air-quality-monitoring sites (*yellow squares*), relevant meteorological observation sites (*green pentagons*) operated during Joint Urban 2003, and Oklahoma Mesonet sites (*red triangles*). The *blue lines* show major roads, *black areas* correspond to lakes, and the *black line* shows the Oklahoma City (OKC) district

The current study focuses on testing the hypothesis that nocturnal mixing processes, which are affected by LLJ development, also strongly influence urban O_3 concentrations. We have thus chosen the same study area (OKC metropolitan area) and period (July 2003) as Hu et al. (2013b) and identified episodes with characteristic LLJ and ozone air-quality signatures, which were studied in detail using Weather Research and Forecasting with Chemistry (WRF/Chem) numerical simulations. More information about the study area and the datasets analyzed is provided in Sect. 2, and the setup of the numerical simulations with WRF/Chem is described in Sect. 3. The general pollution and meteorological patterns observed during July 2003 in the OKC metropolitan area are discussed in Sects. 4.1 and 4.2, with Sect. 4.3 including the WRF/Chem results and detailed analysis of three selected episodes. A summary and conclusions are given in Sect. 5.

2 Study Area and Available Datasets

The selected study area focused on central Oklahoma and included the OKC metropolitan area (Fig. 1). In this region, high O_3 concentrations are often observed in the summertime, primarily during stagnant, high-pressure weather systems with clear-sky conditions and daytime temperatures peaking above 35 °C (Kastner-Klein et al. 2002). Typically during these types of weather systems, southerly winds prevail and signatures of strong LLJs have been observed at night (Wexler 1961; Zhong et al. 1996; Whiteman et al. 1997; Higgins et al. 1997;

Parish and Oolman 2010; Lundquist and Mirocha 2008). The known climatology of these conditions and the flat, homogenous terrain were critical for choosing this domain. During the Joint Urban 2003 (JU2003) tracer experiment (Allwine 2004), conducted from 28 June through 31 July 2003, numerous instrumentation systems were deployed across the OKC metropolitan area including sonic measurements on two tall towers (Grimmond et al. 2004; Gouveia et al. 2007), and sodar and wind profiler measurements (De Wekker et al. 2004) that quantified the structure, dynamics, and mixing in the NBL. July 2003 was thus selected as the study period.

To assess the air quality in the OKC metropolitan area during July 2003, O_3 and NO_x time series measured at six regulatory monitoring sites in the greater OKC area (Fig. 1) were analyzed. Four of the sites are along a 50-km long, north–south oriented transect, beginning with the Goldsby site located in a rural environment south of the OKC metropolis, followed by the suburban site in Moore, Oklahoma, the central OKC site near the urban core, and the North OKC site, which is in suburban terrain. The two other sites are located 23 km west (Yukon) and 17 km east (Choctaw) of the central OKC site. The concentration time series collected at these sites were provided by the Department of Environmental Quality in OKC and included hourly O_3 concentrations at six sites. NO_x concentration data were only available for the central OKC and North OKC site. Unless otherwise stated, all times provided in the remainder of the paper refer to local time (CDT for July in OKC).

Data measured at 80 m a.g.l. with a sodar, which was operated by the Pacific Northwest National Laboratories (PNNL) and located approximately 2.5 km south of downtown OKC during JU2003 (Allwine 2004; De Wekker et al. 2004), were used to determine the prevailing wind direction and wind speed. Additionally, wind speed and wind direction, as well as heat and momentum fluxes, all measured with sonic anemometers at two levels (37.3 and 79.6 m) at the Tyler Media (TM) tower, were also analyzed. This tower was operated by the University of Indiana and located 5.5 km south of the OKC central business district (Grimmond et al. 2004). Based on the TM tower sonic measurements, the flux Richardson number Ri_{fl} was calculated according to

$$Ri_{fl} = -\frac{g}{T_s}\frac{\overline{w'T_s'}}{(du/dz)u_*^2}, \tag{1}$$

where all data were collected at the 37-m level, g is the acceleration due to gravity, T_s the sonic temperature, $u_* = \sqrt{\overline{u'w'}}$ the friction velocity determined from the momentum flux measurements, and $\overline{w'T_s'}$ is the kinematic heat flux. The wind-speed gradient was estimated as $du/dz \approx \Delta u/\Delta z = u_{37}/z$. In addition to the friction velocity u_*, the standard deviation of the vertical velocity fluctuations σ_w observed at the 37-m level was also used as a turbulent velocity scale.

To assess whether data collected at operational meteorological surface networks could serve as an indicator of the nocturnal mixing processes, data from three Oklahoma Mesonet sites located in the OKC metropolitan area (Fig. 1) – Norman (NRMN), Minco (MINC), and Spencer (SPEN) – were analyzed. Information about the typical layout of Oklahoma Mesonet sites and instrumentation used at these sites can be found in McPherson et al. (2007). Since Hu et al. (2013b) concluded that the inversion strength at Oklahoma Mesonet sites could serve as an indicator for mixing within the NBL, it was also used in the current study. The inversion strength can be computed according to

$$\frac{dT}{dz} = \frac{T_9 - T_{1.5}}{9 - 1.5} = \frac{T_9 - T_{1.5}}{7.5}, \tag{2}$$

where T_9 and $T_{1.5}$ are air temperatures measured at 9 and 1.5 m a.g.l. Additionally, it was also tested whether the wind speed V_2 measured at 2 m a.g.l. provided information about mixing within the NBL. Unless otherwise stated, average Mesonet data, computed using data from the NRMN, MINC, and SPEN sites, are presented hereafter.

The LLJ properties and its effect on turbulent mixing during JU2003 were investigated by Lundquist and Mirocha (2008) using data from a boundary-layer wind profiler, which was operated and maintained by PNNL and located approximately 2 km south–south-west of the OKC downtown area. The presence of a LLJ was defined if (1) the wind speed in the lowest 1,000 m increases after sunset, attaining a maximum wind speed typically between 0200 and 0500 CDT, and (2) the maximum wind speed in a profile surpasses a threshold of 10 ms^{-1} [category LLJ-0 in Whiteman et al. (1997) and Song et al. (2005)], with a decrease above the wind-speed maximum of at least 5 m s^{-1}. Using these criteria, of the 27 nights examined, only four nights (July 1, 11, 12, and 23) did not show LLJ signatures in the observed wind profiles. However, the PNNL wind profiler (Lundquist and Mirocha 2008) datasets do not provide wind speeds for the lowest 300 m and LLJs with a wind-speed maximum below this limit can thus not be accurately detected. In the present study, we thus also used data from the ANL wind profiler, which was located approximately 5 km north of OKC downtown (Fig. 1) and provides coverage from 82 to $\approx$ 2,700 m (De Wekker et al. 2004).

3 Three-Dimensional Simulations

For three two-day-long episodes (July 7–8, 17–18, and 25–26) the impacts of the NBL structure and mixing within the NBL on nocturnal O_3 concentrations were further investigated using three-dimensional simulations with WRF/Chem model version 3.4.1 (Skamarock et al. 2008). These three episodes were selected as study periods after analyzing air quality data and JU2003 meteorological data for the whole month of July 2003 (Sect. 4.1). Two one-way nested domains (Fig. 2) with horizontal grid spacing of 22.5 and 4.5 km were used in these simulations. Each domain had 48 vertical layers extending from the surface to 100 hPa. The lowest 20 model sigma levels and corresponding midlevel heights are given in Table 1. For the initial and boundary conditions of all meteorological variables, the $1° \times 1°$ National Centres for Environmental Prediction (NCEP) Final (FNL) Global Forecast System (GFS) analyses are used. The initial and boundary conditions for the chemical species are extracted from the output of the global model MOZART4 with a resolution of $2.8° \times 2.8°$ (Emmons 2010). A summary of the parametrization schemes chosen for the simulations is given in Table 2. The simulations are initialized at 0000 UTC on the first day of each episode and ended 54 h later, and for each simulation, only results starting at midnight local time are included in the comparison.

4 Results

4.1 General Air-Quality Trends During July 2003

To analyze the spatial and temporal variability of O_3 air quality within the study area, daily mean concentrations, daytime maximum concentrations (maximum O_3 value recorded between 0600 and 1800), and nighttime minimum concentrations (minimum O_3 value recorded between 2100 and 0600) for the six monitoring sites in the OKC metropolitan area (Fig. 1) are compared in Fig. 3. The definition of the time windows for the three daily

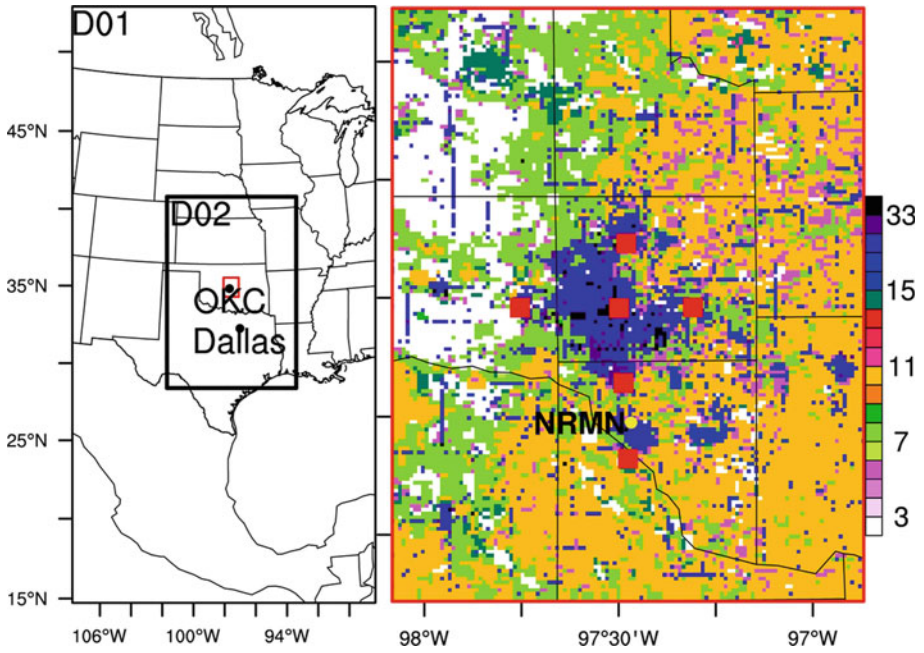

Fig. 2 Domain for WRF/Chem numerical simulations used in this study (*left*). The land-use categories as defined in Hu et al. (2013b) within the *red box* around Oklahoma City (OKC) are zoomed in on *right*. The locations of the six EPA sites in the OKC metropolitan area shown in Fig. 1 are indicated by the *red squares*, and the Norman Mesonet site (NRMN) is marked by a *yellow circle*

O_3 characteristics was based on the sunrise and sunset times for the study area and period, which varied between 0618–0637 and 2049–2036, respectively. Additionally, the observed trends in the time series of hourly O_3 concentrations, which are shown in Figs. 4 and 5 and discussed in more detail below, were also taken into account. Monthly averages of these three daily concentration parameters, shown as bar graphs in Fig. 3, best highlight the spatial variability within the study area. The monthly averages of the daily mean and daytime maximum O_3 concentrations at the six sites varied by less than 7.1 ppb ($\approx$ 18 %) and 5.3 ppb ($\approx$ 9 %). Larger differences can be noted for the nighttime minimum concentrations with the monthly averages varying by 11.9 ppb ($\approx$ 63 %), respectively. The daily mean and nighttime minimum concentrations increased along the south–north transect (from Goldsby to North OKC). At the sites east (Choctaw) and west (Yukon) of the OKC city limits the daily mean concentrations were comparable to the OKC site but slightly lower than for North OKC. The highest nighttime minimum concentrations were observed east of OKC at the Choctaw site. Similar trends can also be observed for the daytime maximum concentrations. Interestingly, the daytime maxima observed at the rural site, Goldsby, were slightly higher than at the suburban site Moore, but the monthly averages differed by < 1 ppb.

For the further analysis only two monitoring sites, OKC and North OKC, were chosen. The temporal variability during July 2003 was high with the daily mean O_3 concentrations at the OKC and North OKC sites (average values based on data recorded at these two sites) varying between 25–57 ppb ($\approx$ 55 %), the daytime maxima between 33 and 88 ppb ($\approx$ 63 %), and the nighttime minima between 7 and 42 ppb ($\approx$ 83 %). When comparing the range of values and time series (Fig. 3) for the three concentration statistics it can be noted that the nighttime minimum concentrations often remained elevated, with values above 20 ppb

Table 1 Sigma levels and corresponding midlevel heights of lowest 20 model layers

Sigma level	Midlevel height (m a.g.l.)
1	12
0.997	37
0.994	61
0.991	86
0.988	111
0.985	144
0.975	186
0.97	227
0.96	290
0.95	374
0.94	459
0.93	545
0.92	631
0.91	717
0.895	826
0.88	958
0.865	1092
0.85	1226
0.825	1409
0.8	1640

Table 2 Overview of parametrization schemes selected for WRF/Chem simulations

Parametrized process	Chosen scheme	Reference
Shortwave radiation	Dudhia algorithm	Dudhia (1989)
Longwave radiation	Rapid radiative transfer model (RRTM)	Mlawer et al. (1997)
Microphysics	WRF single-moment 6-class (WSM6) scheme	Hong et al. (2004)
Planetary boundary layer	Yonsei University (YSU) scheme	Hong et al. (2006)
Land surface	Noah land-surface scheme	Chen and Dudhia (2001)
Gas-phase chemical reactions	Regional Atmospheric Chemistry Mechanism (RACM)	Stockwell et al. (1997)
Anthropogenic emissions of chemical species	Hourly values from 4 km × 4 km national emission inventory (NEI) for year 2005	
Biogenic emissions	Algorithms established by Guenther et al.	Guenther et al. (1994)

(15 days). Improving the physical understanding about relevant processes contributing to these elevated nocturnal concentration levels motivated the current study.

4.2 Links Between Meteorological and Pollution Patterns During July 2003

To identify possible links between the observed temporal variability of O_3 concentrations and meteorological parameters, diurnal cycles of O_3 and NO_x concentrations, prevailing

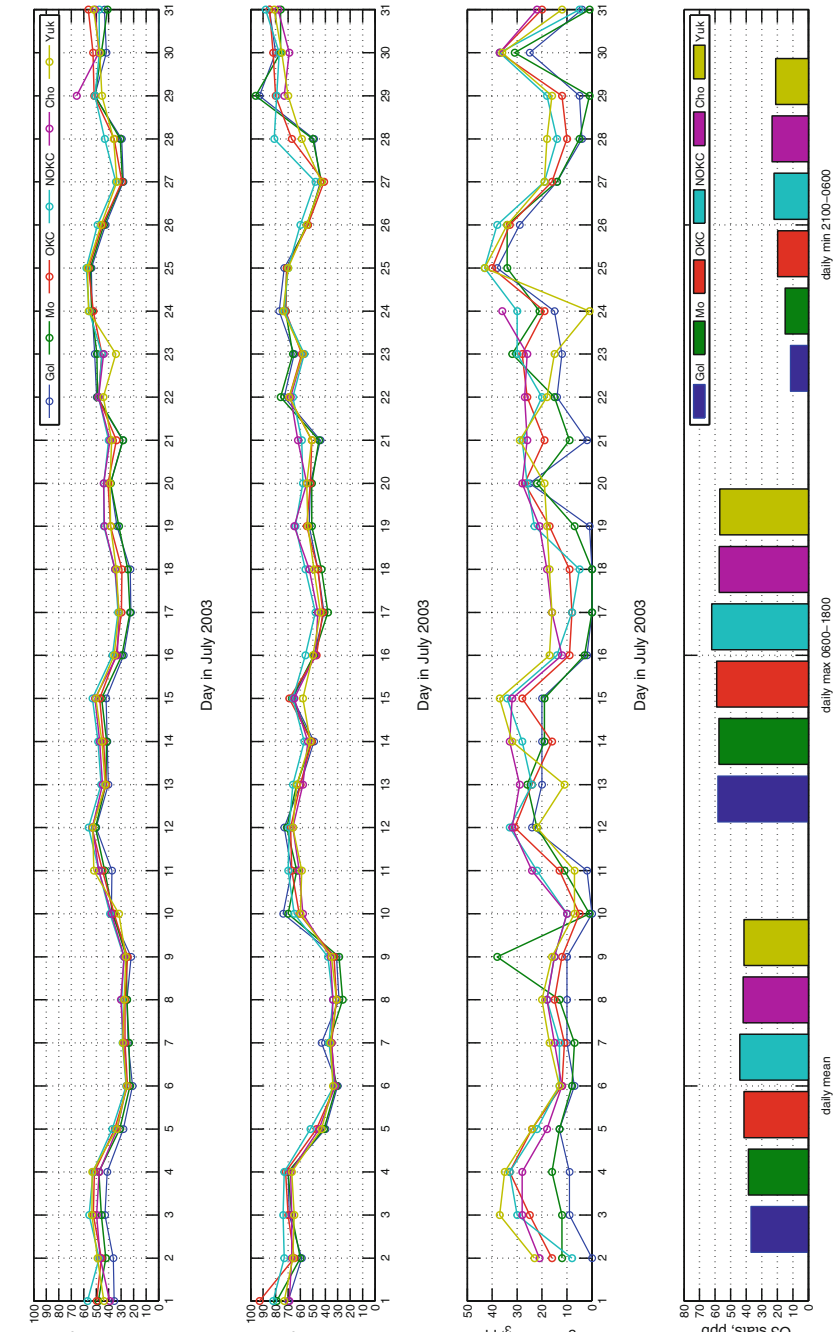

Fig. 3 Ozone concentration statistics at the six monitoring sites Goldsby (*blue*), Moore (*green*), OKC (*red*), OKC North (*teal*), Choctaw (*pink*), and Yukon (*yellow*) during July 2003: **a** daily mean, **b** daytime maximum (0600–1800), **c** nighttime minimum (2100–0600), and (**d**) monthly averages of these three concentration statistics

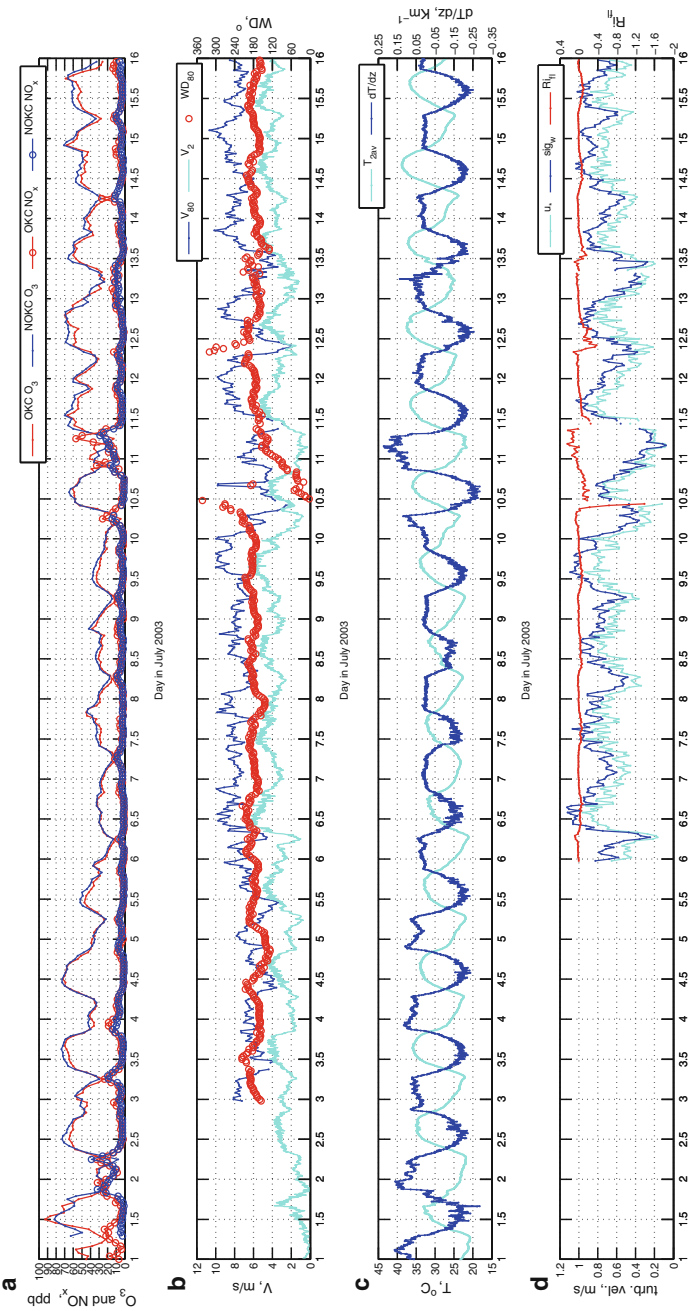

Fig. 4 O_3 (*solid lines*) and NO_X (*circles*) concentrations at two EPA monitoring sites in the OKC metropolitan area (*red* OKC, *blue* North OKC) during July 7–16, 2003 (**a**). Wind direction (TM tower at 80 m, *red* right axis) and wind speeds (*left* axis) at 2 m (average of 3 Mesonet sites, *teal*), and 80 m above ground level (a.g.l., TM tower, *dark blue*) are plotted in (**b**). Plot (**c**) shows the average air temperature at three NRMN (*teal* left axis) along with the average vertical temperature gradient dT/dz (*blue* right axis). The friction velocities u_* (*teal* left axis) and vertical turbulent velocities σ_w (*blue* left axis) are shown in (**d**) together with the flux Richardson number Ri_{fl} (*red* right axis)

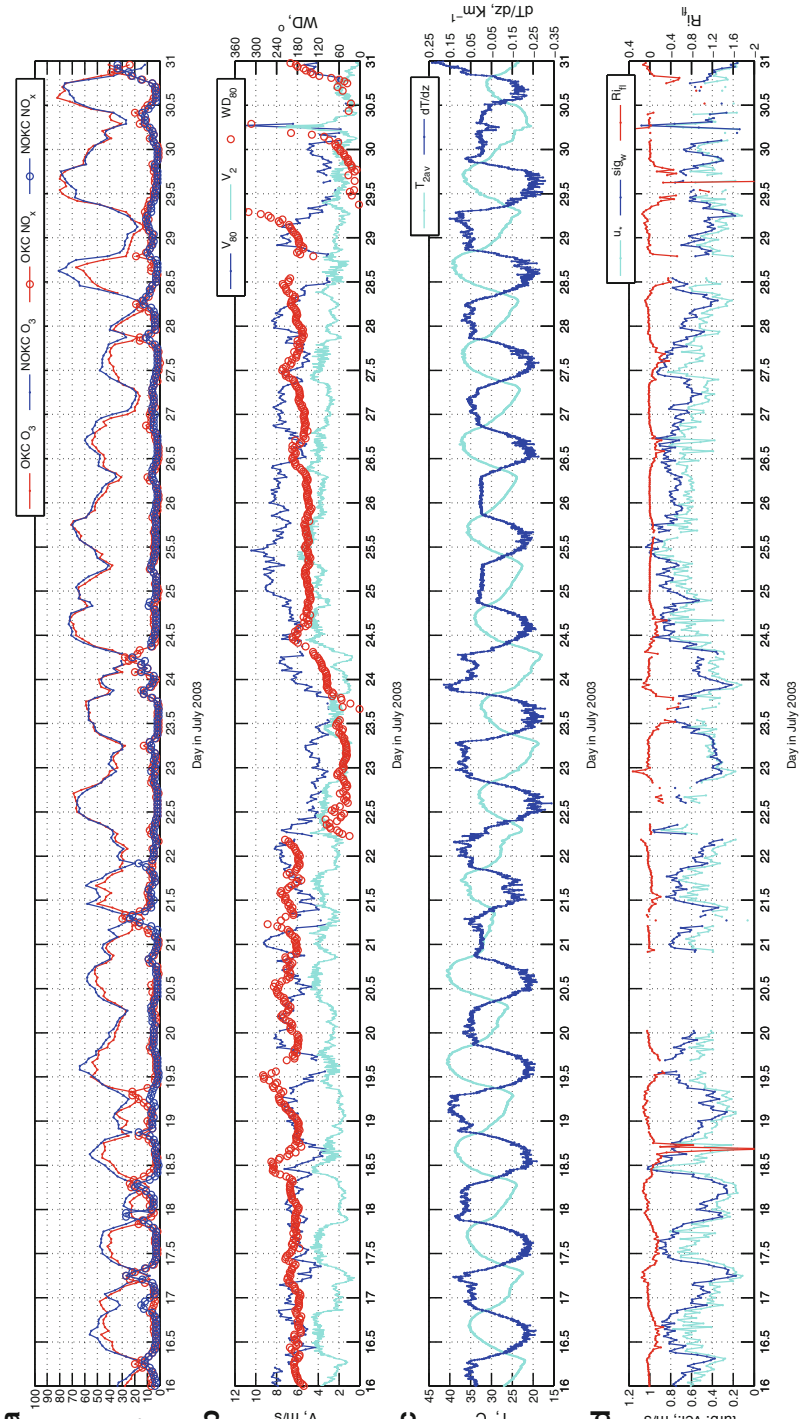

Fig. 5 Same as Fig. 4 but for July 16–31, 2003

wind directions, wind speeds, turbulent velocity scales, and stability parameters are shown in Figs. 4 and 5 for July 2003. Marked differences between weekend and workdays were not observed. As expected, the highest O_3 concentrations are typically observed in the afternoon with peak values near 80 ppb. After sunset, O_3 concentrations start to decline, but the diurnal cycles reveal that secondary O_3 peaks are often observed after sunset (at 2100 or later). These trends formed the basis for defining the maximum daytime concentration between 0600 and 1800 along with the nighttime minimum concentration between 2100 and 0600 as two important daily concentration characteristics, as discussed earlier. There is no indication that the nocturnal O_3 peaks are directly linked to NO emissions during the evening rush hour. In fact, there is a tendency that preceding daytime (0600–1800) and concurrent nighttime (2100–0600) maximum NO_x concentrations are higher during the night with minimum O_3 concentrations below 20 ppb. These tendencies could be interpreted as higher NO emissions causing stronger O_3 titration at night, which is plausible. However, the scatter is fairly large, and clear correlations between NO_x and O_3 statistics were not observed, which may also be explained by the lack of separate NO and NO_2 measurements. Furthermore, higher NO_x values during nights with low O_3 concentrations are also an indication for accumulation of NO within a stable shallow surface layer (Geyer and Stutz 2004a,b).

The wind-direction data show that winds were primarily from the south during July 2003, except for July 10 and 29, when frontal passages occurred, and during July 22–24, when winds were primarily from the east–north-east. Near-surface air temperatures also varied throughout the month, with the daily minimum temperatures ranging from 18 to 28 °C and the daily maximum temperatures from 31 to 41 °C. Lower temperatures were observed at the beginning of the month and after the winds shifted to the east–north-east on July 22. The wind speeds V_2 recorded at 2 m a.g.l. show the typical diurnal cycle, with wind speeds decreasing to much lower values after sunset. The daily maximum wind speeds ranged between 3.4 and 7.8 m s^{-1}, while the minimum values ranged between 0 and 3.1 m s^{-1}, with an average value of 1.44 m s^{-1}.

By comparing the wind speed and O_3 concentration time series, correlations between nocturnal values of these two parameters can be noted: during nights with relatively strong sustained nocturnal winds, such as during July 25–28 (Fig. 5), O_3 concentrations were elevated at night, while during nights with calm periods, such as during July 16–19 (Fig. 5), concentrations showed a marked decrease at night. The friction velocity u_* and standard deviation of the vertical velocity fluctuations σ_w, which are both parameters that describe the intensity of turbulent vertical mixing, follow the trends of wind speed, which indicates that during nights with higher surface wind speeds, mixing within the NBL was stronger. Accordingly, lower values of the flux Richardson number Ri_{fl} (1) and near-surface inversion strength $\mathrm{d}T/\mathrm{d}z$ (2) were observed during nights with higher surface wind speeds and O_3 concentrations.

Similarly to the findings of Hu et al. (2013b), who concluded that $\mathrm{d}T/\mathrm{d}z$ could be used as an indicator of the intensity of mixing processes within the NBL, it appears that the near-surface inversion strength can also serve as an indicator for nocturnal O_3 concentration levels. During nights with a strong inversion (large $\mathrm{d}T/\mathrm{d}z$) mixing within the NBL is very limited, and O_3 trapped within the decoupled, the shallow stable surface layer is depleted due to NO titration reactions. In contrast, active downward mixing of O_3 during nights with weak inversions (small $\mathrm{d}T/\mathrm{d}z$) compensates the depletion of O_3 near the surface, and O_3 concentrations remain elevated at night. However, while Hu et al. (2013b) found that the nocturnal UHI value correlated well with parameters that characterize mixing within the NBL, O_3 concentrations are not only influenced by local meteorological conditions but also strongly depend on the emission rates of anthropogenic and biogenic precursor pollutants, chemical reactions rates,

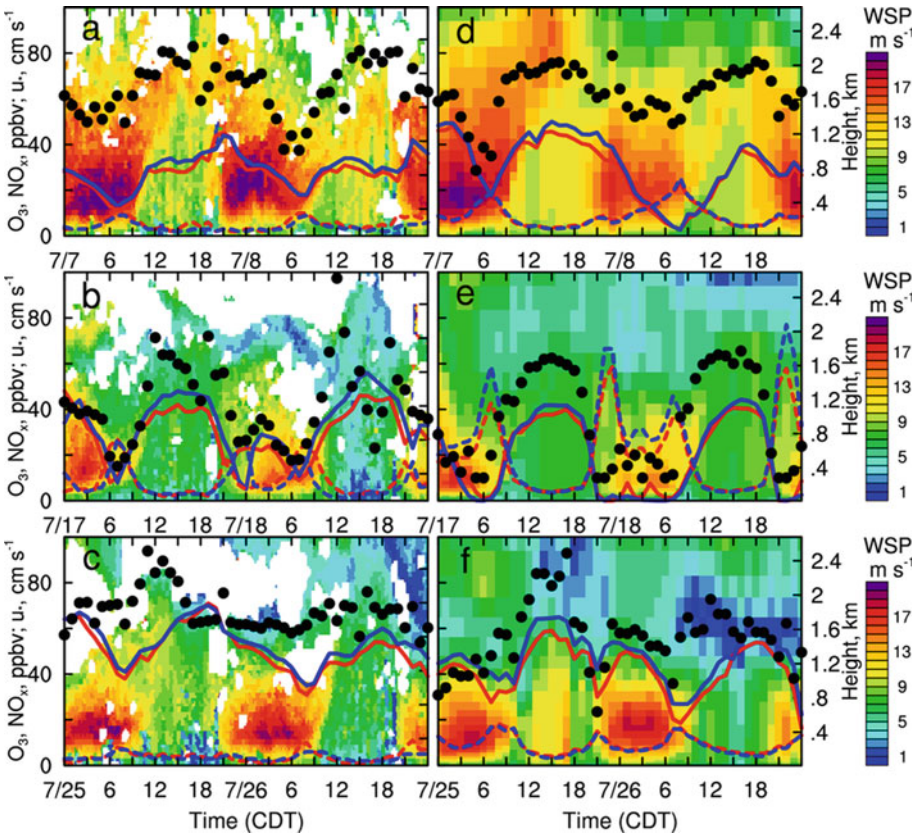

Fig. 6 Wind profiles at Argonne National Laboratory (ANL) site (*colour map*), together with O_3 (*solid lines*) and NO_X (*dashed lines*) concentrations at OKC (*red*) and NOKC (*blue*) monitoring sites, during three selected episodes. The *black dots* show the observed and simulated friction velocities at the TM tower (to fit the axis scale cm s^{-1} was chosen as the unit friction velocities in these plots). Observations (**a**–**c**) are compared against the corresponding WRF/Chem simulation results (**d**–**f**)

and advection of O_3 and its precursor pollutants at various heights within the atmosphere (Geyer and Stutz 2004a,b). It is thus rather difficult to directly correlate nocturnal O_3 concentrations with meteorological parameters, and the limited information of chemistry data (only surface observations of O_3 and NO_x at a limited number of sites) further complicates a more in-depth analysis of the observations. The role of LLJs in promoting mixing and downward transport of O_3 was thus further investigated with the three-dimensional air chemistry model WRF/Chem.

4.3 Results of WRF/Chem Simulations for Three Selected Episodes

To further investigate how NBL structure and dynamics influence O_3 pollution levels at night, three 2-day episodes were selected for a more detailed analysis using also numerical model fields from WRF/Chem simulations. A comparison of measured and WRF/Chem simulated near-surface O_3 and NO_x concentration time series for the three episodes is shown in Fig. 6. The colour map in the background of the plots illustrates the magnitude of measured and

simulated wind speeds up to 2.8 km a.g.l., whereby the measured data stem from the ANL wind profiler, which was continuously operated during JU2003. To illustrate the turbulent mixing properties, observed and simulated friction velocities u_* at 37 m a.g.l. at the TM tower site are also plotted.

Episode 1 (July 7–8) was selected because the O_3 time series show pronounced maxima occurring just after sunset followed by a rather slow concentration decline throughout the night (Fig. 6a). While the O_3 concentrations were generally rather low during episode 1, it is an interesting study period as the nighttime minimum concentration on July 8 was only 50 % lower than the daytime maximum on July 7. Friction velocities u_* remained high after sunset on July 7 and only dropped down to ≈ 0.4 m s^{-1} near sunrise on July 8. As seen in Fig. 4, surface wind speeds V_2 remained above 2 m s^{-1} and surface inversions $\mathrm{d}T/\mathrm{d}z$ below 0.02 K m^{-1} throughout both nights.

Episode 2 (July 17–18) represents days during which an O_3 peak/plateau is observed in the afternoon (before 1800). During the first night, O_3 concentrations consistently declined, dropping to levels below 10 ppb before sunrise on July 17 (Fig. 6b). After sunset on July 17 the O_3 concentrations also declined rapidly but remained above 20 ppb throughout the night and a secondary maximum was observed after midnight in the early morning hours of July 18. This secondary maximum corresponds to a slight increase in u_*. Compared to episode 1, friction velocities u_* were, however, clearly lower, and surface winds/inversion strength were lower/higher, with a surface wind speed of $V_2 < 1$ m s^{-1} and inversion strength $\mathrm{d}T/\mathrm{d}z$ becoming close to 0.15 K m^{-1} before sunrise on July 17 (Fig. 5).

Episode 3 includes the 48-h time period consisting of July 25–26. During both nights, O_3 concentrations remained above 30 ppb and after sunset on July 25, the friction velocity u_* remained above 0.6 m s^{-1} throughout the night (Fig. 6c). Nocturnal $\mathrm{d}T/\mathrm{d}z$ values are comparable to those observed during episode 1 (Fig. 5). During episode 3, pollution levels were overall highest compared to the two other episodes, whereby the daily concentration peaks occurred later than during episode 2 but earlier (before sunset) than during episode 1.

The prevailing wind directions were quite similar during all three episodes, with primarily southerly winds occurring. Air temperatures were similar during episodes 2 and 3 but lower during episode 1, which could partially explain the trend toward lower O_3 concentrations during that episode. A positive correlation between air temperature and surface O_3 concentrations has been observed in numerous studies (e.g., Kastner-Klein et al. 2002) and can be explained by several factors including increasing emission rates for certain precursor pollutants as well as air temperature being an indicator for enhanced solar radiation and the presence of high-pressure stagnation systems (Bloomer et al. 2010). The emission data used were identical for the simulations of all three episodes. Any observed differences between simulations for the three episodes were thus caused by differences in meteorological patterns and cannot be explained by variations in the emission rates.

A direct comparison of simulated and measured O_3 concentrations and their rates $\mathrm{d}O_3/\mathrm{d}t$ at the OKC site are shown in Fig. 7 together with time-height plots of simulated O_3 concentrations and simulated boundary-layer heights. The agreement between measured and simulated O_3 concentrations and wind speeds is overall fairly good as the general trends are reproduced for all three episodes. Differences can, however, be noted in the timing of the daytime O_3 buildup (primarily for episodes 1 and 3), with WRF/Chem predicting earlier concentration peaks than what is observed. At night, observations and simulation results also deviate, which is discussed in more detail further below. Larger differences between observations and simulations can be noted for the NO_x concentrations. The WRF/Chem simulations predict values that are roughly twice as high as the observations. The general trends of higher NO_x concentrations within a shallow, stable boundary layer (episode 2, Figs. 6e

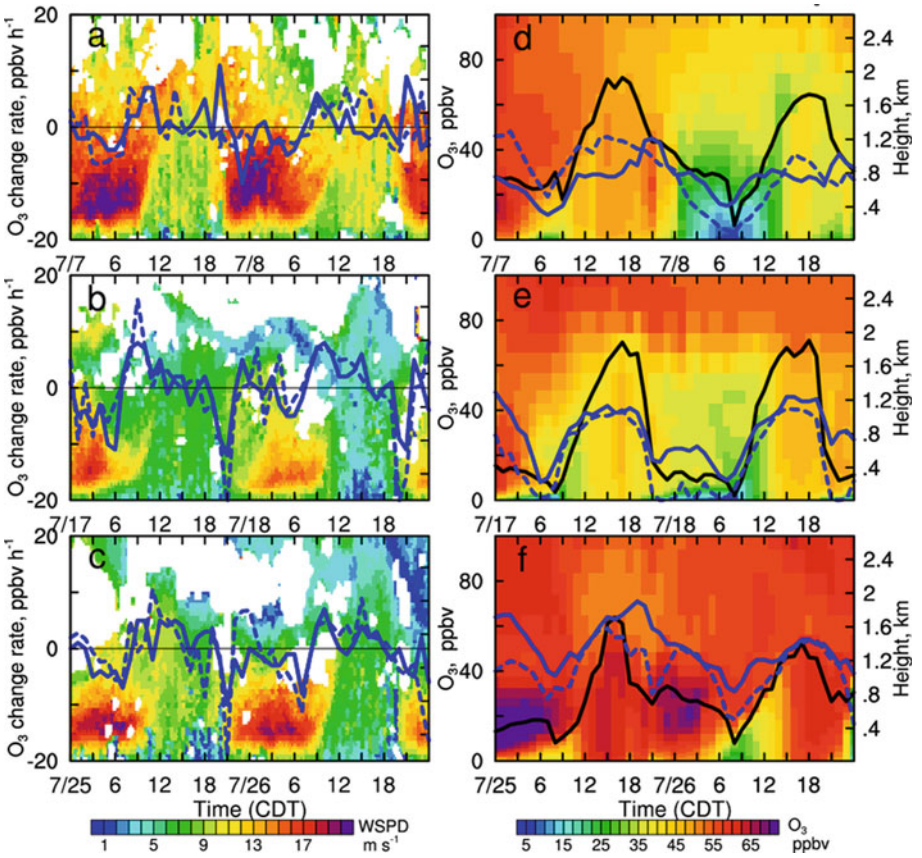

Fig. 7 ANL wind profiles (*colour* map) together with measured (*blue solid line*) and simulated concentration rates dO_3/dt (*blue dashed line*) at OKC monitoring site during three selected episodes (**a**–**c**). Additionally, observed (*blue solid line*) and simulated (*blue dashed line*) O_3 concentrations at OKC site are plotted together with simulated boundary-layer heights (*black*) and a time-height plot of simulated ozone concentrations (**d**–**f**)

and 7e), within which surface O_3 concentrations decrease rapidly, are, however, captured by the simulations.

Among the three episodes, clear differences can be noted in the wind profiles at night, with strong LLJs developing quickly after sunset (at around 2000 hours) during episodes 1 and 3, while during episode 2 a much weaker jet is observed several hours later (at around 2300). The timing and strength of the LLJ appears to be strongly correlated with the O_3 concentration level observed near the ground at night. During nights with an early onset of a strong LLJ (episodes 1 and 3), during which mixing persists (Fig. 6), boundary-layer heights remained high and only decreased to less than 400 m around sunrise (Fig. 7). For such deep NBL, surface O_3 concentrations decreased slowly and generally remained elevated. In the case of the weak, later LLJ (episode 2), the boundary layer was less than 400 m deep throughout most of the night and surface ozone showed the expected fast decrease after sunset (Fig. 7e). While the overall trends in dO_3/dt are well captured by WRF/Chem, the model fails to reproduce particular features of the individual episodes such as the increase of ozone during 1800–2100 hours on July 7 and the increase in the early morning hours of

July 18 related to the late LLJ development. Also, during 2100–0000 hours on July 25, the model predicted a concentration increase, while the O_3 observations steadily declined. A number of factors could contribute to these differences in observed and simulated nocturnal concentration values and trends, including model errors associated with vertical mixing of chemical species (Pleim 2011; Hu et al. 2012), uncertainties in the emission factors at the regional scale that might cause differences in the upper layer concentration values, and the strength of the elevated O_3 advection by the LLJ. The time-height concentration plots (Fig. 7) nicely illustrate that in the simulations elevated advection of O_3 did play a role during episode 3. Simulated O_3 concentrations between 400–1,000 m increase after 2100 on July 25 (Fig. 7f), which can only be explained by advection.

To further evaluate the WRF/Chem model results, spatial O_3 concentration distributions for the lowest model level at 0000 CDT on the second night of each of the three episodes are compared with observations in Fig. 8a–c. The spatial patterns generally agree well with the observed trends. For individual sites, the model predictions deviate from the observations, which can be expected as some measurements sites might be strongly influenced by local emissions that are not accurately resolved in the model. When comparing the three episodes, it becomes very clear that during episode 3 elevated O_3 concentrations were observed over a large area extending from northern Texas through to Michigan, which coincides with a region of high wind speeds at 533 m a.g.l. (Fig. 8f), the height that corresponds to the LLJ nose with peak velocities (Fig. 9c). During this episode, O_3 concentrations were elevated within the region characterized by high jet speeds and upwind (southeast) of central Oklahoma (Fig. 8i), which promoted elevated, long-range transport of O_3 by the LLJ. During episodes 1 and 2, the areas affected by LLJs were much smaller (Fig. 8g, h) and long-range transport of O_3 by the LLJ appeared to play less of a role in the OKC metropolitan area as the concentration levels at the height of the jet nose tended to decrease upwind of the study area (Fig. 8d, e). As can be seen in Fig. 9b, the LLJ was also much shallower during episode 2 than during the other two episodes. While during episodes 1 and 3 (Fig. 9a, c) the level of peak velocities was around 500 m, it was only at approximately 250 m a.g.l. during episode 2 (which is why a different layer is shown in Fig. 8e, h for episode 2).

The comparison of observed (o) and simulated (s) wind profiles, also shown in Fig. 9, is overall very good. To present a quantitative evaluation, the observed wind profiles were interpolated to the same grid used in the simulations, and statistical performance parameters were computed using the six wind profiles for each episode (Table 3). For all three episodes, the comparisons of the average (data from all profiles up to 2 km height were included) observed ($U_{o,av}$) and simulated ($U_{s,av}$) wind speeds are very similar (differences range between 4 and 8 %), which is also true for the corresponding maximum ($U_{o,max}$ and $U_{s,max}$) and minimum ($U_{o,min}$ and $U_{s,min}$) wind-speed values. However, during episode 1 the WRF simulations underestimate the maximum wind speeds, while during episode 3 maximum wind speeds are overpredicted and the simulated minimum wind speeds are lower than the observed values. The average ($[U_s/U_o]_{av}$), maximum ($[U_s/U_o]_{max}$), and minimum ($[U_s/U_o]_{min}$) ratios of simulated to observed wind speeds are overall acceptable with the best agreement for episode 1, followed by episode 2 and then 3. The corresponding factor of two values (FA2) range between 100 % (episode 1) and 93 % (episode 3). The bias, FB, and NMSE further confirm that the model predicted the wind speeds during episodes 1 and 2 very well, and that model performance was only slightly worse for episode 3.

The joint analysis of the wind and O_3 profiles throughout the nights (Fig. 9) provides further insight into how the structure and development of the LLJ impact nocturnal air quality. During episode 1 (Fig. 9a), a strong and deep LLJ develops after sunset (for 2200 the simulations show a clear jet profile) and persists throughout the whole night (by 0700 the predicted jet

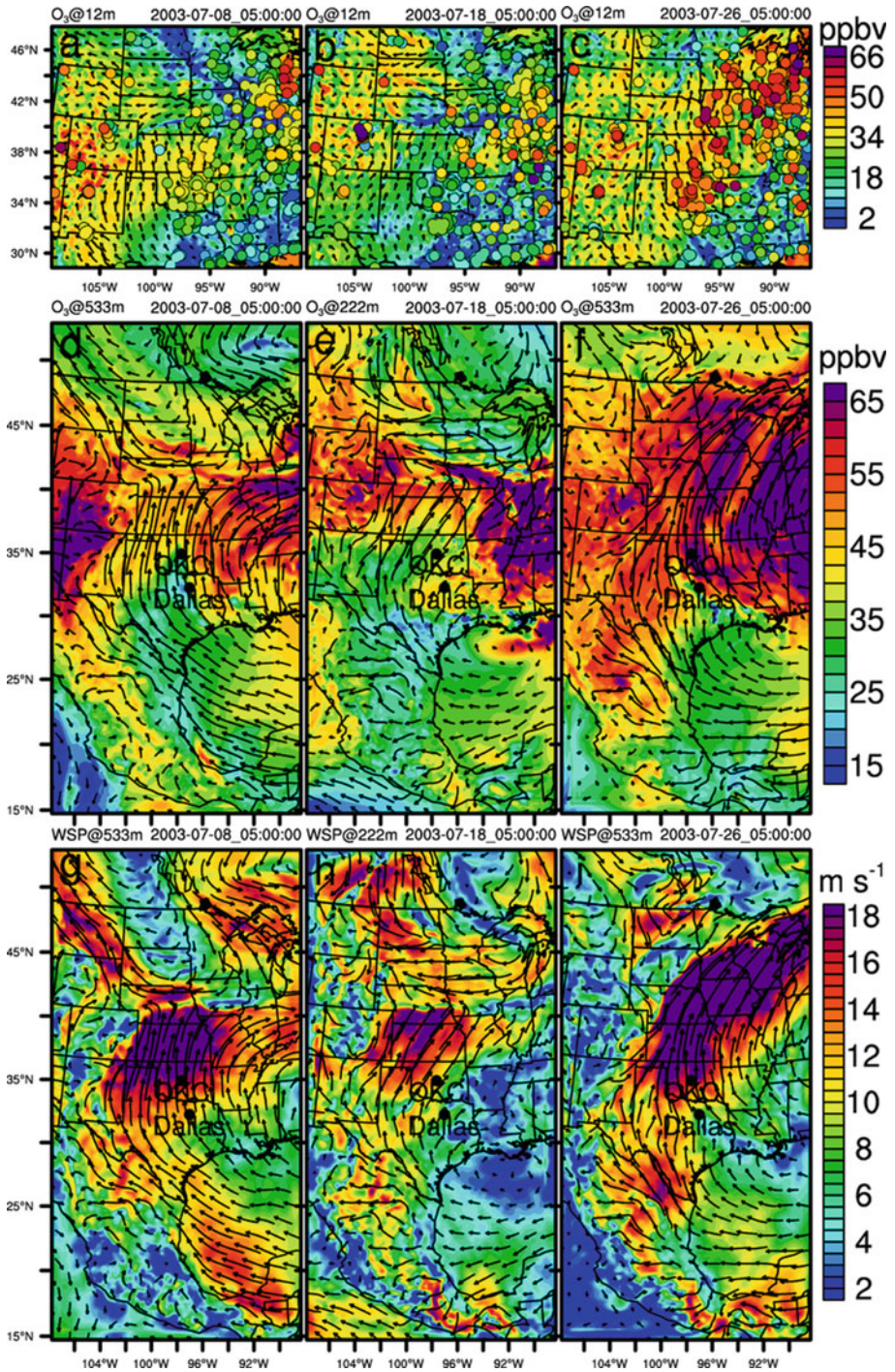

Fig. 8 Comparison of simulated near-surface O_3 concentrations (**a**–**c**) with observations (*circles*); and O_3 concentrations (**d**–**f**) and wind speeds (**g**–**i**) predicted by WRF/Chem at the height of the LLJ nose. The results correspond to 0000 CDT on July 8 (**a**, **d**, **g**), 18 (**b**, **e**, **h**), and 26 (**c**, **f**, **i**)

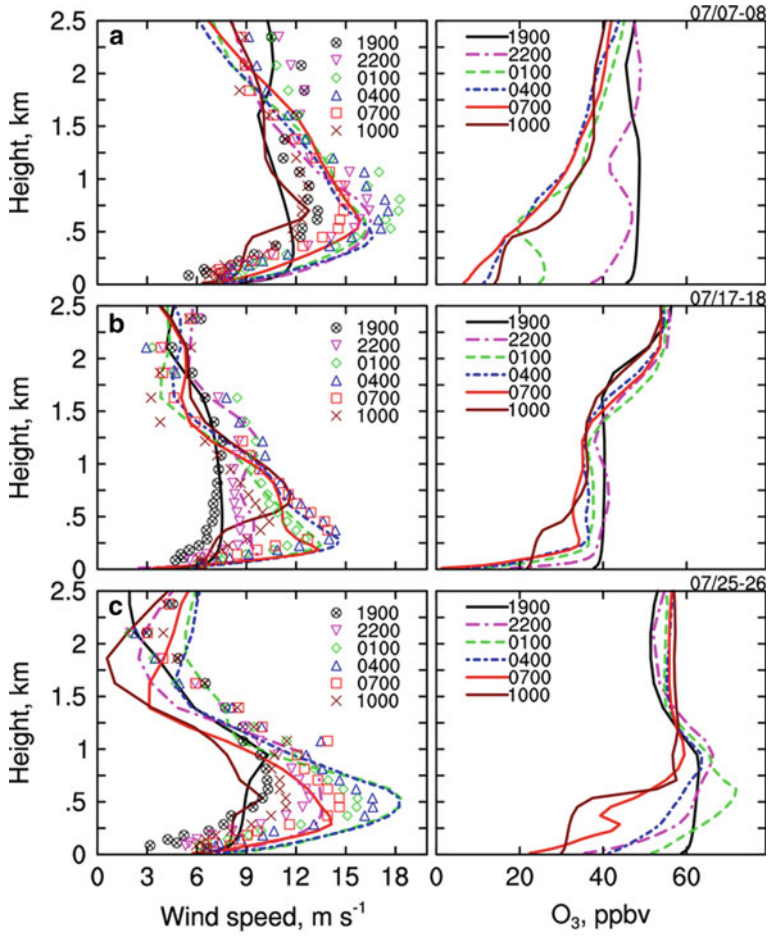

Fig. 9 Vertical wind and O_3 profiles predicted by WRF/Chem for the time period 1900 to 1000 during the nights on July 7–8 (**a**), 17–18 (**b**), and 25–26 (**c**). The *symbols* shown in the *left* plots correspond to the observed wind profiles at the ANL site

is still very strong). The vertical gradients of O_3 are very small during this episode, which indicates that O_3 is actively mixed within a deep NBL. At the surface, O_3 titration is partially compensated by the downward transport from higher elevations, which results in a slow but more gradual reduction of O_3. During episode 2, a weaker and shallower LLJ develops between 2200 and 0100 (Fig. 9b). The simulated O_3 profiles have marked gradients with a strong O_3 reduction near the ground: by 2200 surface O_3 concentrations are reduced by more than 50 %, and by 0700 surface ozone is fully depleted. However, above 250 m, the height of the LLJ nose, concentration levels are high and remain nearly unchanged (reduction less than 10 ppbv) throughout the night. This vertical structure of the O_3 concentrations agrees with the traditionally expected nocturnal trends in NOx-rich areas under stable conditions with limited vertical mixing (Geyer and Stutz 2004a,b). The strongest LLJ was observed during episode 3 (Fig. 9c). Just as during episode 1, wind speeds peak at approximately 500 m a.g.l. However, the wind profiles show a much larger, negative gradient above the level of peak wind speeds, which results in much lower wind speeds above $\approx$ 800 m than during

Table 3 Statistical model performance parameters computed using observed and simulated wind profiles shown in Fig. 9

Performance parameter	Episode 1	Episode 2	Episode 3
$U_{o,av}$ (m s^{-1})	11.08	7.90	8.52
$U_{o,av}$ (m s^{-1})	11.41	8.13	9.18
$U_{o,max}$ (m s^{-1})	18.26	14.36	16.64
$U_{s,max}$ (m s^{-1})	16.65	14.61	18.31
$U_{o,min}$ (m s^{-1})	5.51	2.95	1.92
$U_{s,min}$ (m s^{-1})	5.54	2.50	0.58
$[U_s/U_o]_{av}$	1.06	1.05	1.13
$[U_s/U_o]_{max}$	1.99	1.74	2.77
$[U_s/U_o]_{min}$	0.66	0.38	0.12
FA2 (%)	100.00	98.61	93.06
Bias (m s^{-1})	0.34	0.23	0.66
Fractional bias (*FB*) (%)	−2.99	−2.88	−7.48
Normalized mean square error (*NMSE*) (%)	3.68	4.63	8.89

episode 1. The LLJ is also less persistent; by 2200 it is not yet fully developed, and by 0700 it has already weakened. The O_3 profiles indicate that the strong LLJ triggered active mixing of O_3 toward the surface. However, as mentioned earlier, elevated long-range transport by the LLJ also seems to play a role during this episode, as the concentration increase at the height of the jet nose (≈500–600 m) at around midnight cannot be explained by chemical production. It appears that O_3 transported by the LLJ is mixed both downward and upward, which results in the simulated ground-level O_3 maximum having a secondary maximum at night and a slight increase in O_3 concentrations above ≈1.2 km. The combination of active downward mixing and elevated O_3 transport contributes to the highest nocturnal surface O_3 concentrations, which in the WRF/Chem fields still remain above 20 ppbv by 0700 during this episode. The observed values at 0700 hours are even higher (≈ 35 pbbv), even though the secondary maximum at midnight predicted by the WRF/Chem simulations is lacking (Fig. 7f).

To further investigate the role of vertical mixing and horizontal advection, the concentration rates dO_3/dt at midnight due to vertical mixing and horizontal advection were computed based on the WRF/Chem model output (Fig. 10). Horizontal advection was evaluated both for the lowest model level and for the height of the LLJ nose. During episode 3, the concentration changes dO_3/dt due to advection at the height of the LLJ nose (Fig. 10i) in central Oklahoma and upwind areas were higher than during the other two episodes (Fig. 10g, h), which confirms that the LLJ supported advection of O_3 during epsiode 3, while the role of elevated advection appears negligible during the other episodes. However, the computed advection rates are spatially rather inhomogeneous, which is even more pronounced near the surface (Fig. 10d–f). Since upper-layer measurements are lacking and the observations near the surface are very sparse, these calculations could also not be evaluated and should thus be interpreted with caution. However, it can be clearly noted that vertical mixing (Fig. 10a–c) affects surface ozone much more than horizontal advection and that clear differences in the strength of vertical mixing emerge among the three episodes. During episode 3, the elevated advection of O_3, along with sustained vertical mixing triggered by a strong LLJ, promotes the strongest downward transport of O_3 to the surface. Earlier in the night (at about 2100,

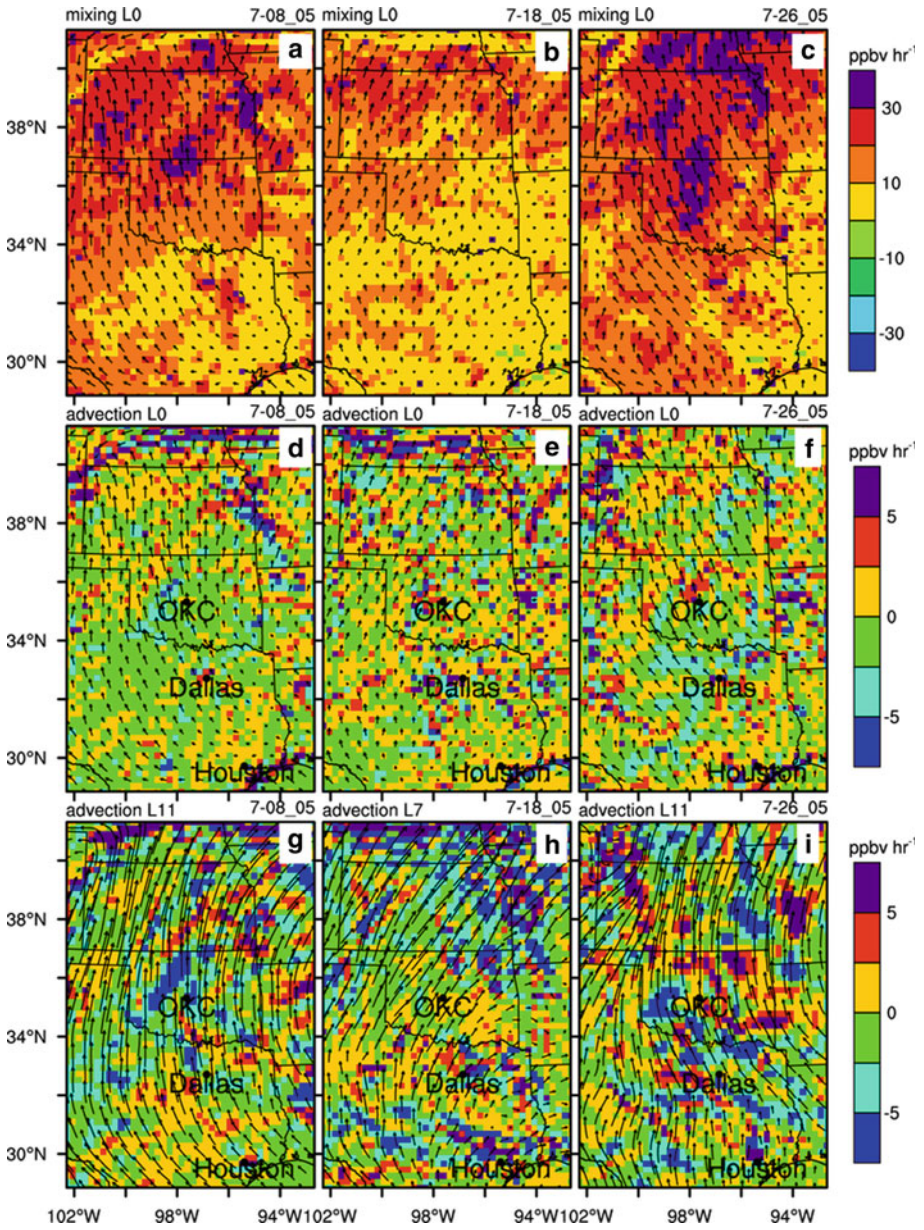

Fig. 10 Simulated concentration rates dO_3/dt due to vertical mixing in lowest model level (**a**–**c**), horizontal advection in lowest model level (**d**–**f**), and horizontal advection at height of LLJ nose (**g**–**i**) at 0000 CDT on July 8 (**a**, **d**, **g**), 18 (**b**, **e**, **h**), and 26 (**c**, **f**, **i**)

not shown), the downward transport of O_3 to the surface is comparable during episodes 1 and 3, but the lack of elevated advection during episode 1 results in declining concentrations and smoother vertical gradients up to 2.5 km (Figs. 7 and 9), which causes reduced vertical transport later at night. During episode 2, the rate of change of O_3 due to vertical transport is

two to three times lower and likely compensated by the combined effects of deposition and chemical reactions (primarily between O_3 and NO) within a shallow surface layer in which surface O_3 concentrations then remain low at night.

5 Conclusions

Ozone concentrations measured at regulatory monitoring sites in the greater OKC metropolitan area and WRF/Chem simulations illustrate the impact of nocturnal mixing and transport regimes on air quality. Datasets collected during the JU2003 campaign provided detailed information about the temporal evolution, vertical structure, and strength of the LLJ in the OKC area. As discussed in the literature (Banta et al. 1998; Zhang and Rao 1999; Reitebuch et al. 2000; Solomon et al. 2000; Philbrick et al. 2003; Geyer and Stutz 2004a,b; Tong et al. 2011; Hu et al. 2013a), elevated O_3 concentrations and secondary, nocturnal peaks are linked to strong mixing and downward transport of O_3 from higher elevations to the surface. Our results confirm these findings and clearly demonstrate the important role of LLJs, a prominent feature in the Southern Great Plains, in promoting persistent mixing and downward O_3 transport in the NBL. A statistical evaluation of the WRF simulations, which was based on observed and simulated wind-speed profiles for the time period from 1800 to 0900, showed that the model reproduced the LLJ structure very well.

The simulations further provided new insights, showing that the timing, strength, and vertical extent of the LLJ strongly influence the O_3 profiles. The highest nocturnal, near-surface O_3 concentrations are found in the case of a strong but vertically confined LLJ that also triggers elevated, nocturnal long-range transport. A strong, persistent, and deep LLJ promotes strong mixing, which results in gradually decreasing O_3 concentrations from the surface throughout the residual layer for the entire night. The lowest near-surface concentrations occur for a weak, shallow LLJ due to limited vertical mixing between the stable surface layer and residual layer. However, in the latter case O_3 concentrations within the residual layer remain relatively high and decline only slowly throughout the night.

Overall, the simulated surface O_3 concentrations agree well with observations. However, while the WRF/Chem numerical model is able to capture general trends, difficulties in reproducing small-scale changes at night can be noted for all three simulated episodes, and the simulated NO_x concentrations are about twice as high as the observed values. An in-depth analysis of possible reasons for these differences and suggestions for model improvements will require profile measurements of additional pollutants along with detailed meteorological observations.

Since O_3 concentration levels are strongly influenced by emission rates and air chemistry, but only limited chemistry observations were available, it is difficult to establish direct correlations between O_3 concentrations and meteorological parameters. However, trends of increasing nocturnal O_3 levels for increasing friction velocities u_* and near-surface wind speeds V_2 but decreasing near-surface temperature inversion $\mathrm{d}T/\mathrm{d}z$ can clearly be noted. As stability increases, near-ground O_3 concentrations decrease due to NO titration reactions that actively deplete O_3 within a shallow, decoupled stable surface layer, while O_3 concentrations remain high and nearly unchanged throughout the night within the residual layer.

Our study demonstrates that detailed meteorological information can provide new insights into nocturnal mixing processes and related air-quality problems, but the lack of vertical concentration profiles still leaves a number of questions concerning the interplay between the ABL structure and air chemistry. Specifically, this lack hinders a more in-depth, quantitative analysis of the ozone budget. More detailed datasets are also essential for evaluating and

improving the WRF/Chem model simulations. Future studies should thus focus on simultaneous, high-resolution measurements of meteorological and air chemistry profiles.

Acknowledgments This study was supported by funding from the Office of the Vice President for Research at the University of Oklahoma and through the NSF Career award ILREUM (NSF ATM 0547882). The JU2003 experiments were funded by the Defense Threat Reduction Agency's Urban Dispersion Modeling program managed by John Pace and Rick Fry. Oklahoma's taxpayers fund the Oklahoma Mesonet through the Oklahoma State Regents for Higher Education and the Oklahoma Department of Public Safety. The authors would also like to thank Leon Ashford from the Department of Environmental Quality in OKC for his support in obtaining the air-quality data, Jeffrey Basara and Brad Illston from the Oklahoma Climatological Survey for providing data from the Oklahoma Mesonet and for creating Fig. 1 for the manuscript, and three anonymous reviewers for their constructive and helpful comments.

References

Acevedo OC, Fitzjarrald DR (2001) The early evening surface-layer transition: temporal and spatial variability. J Atmos Sci 58:2650–2667

Allwine KJ (2004) Overview of JOINT URBAN 2003—an atmospheric dispersion study in Oklahoma City. In: Symposium on planning, nowcasting, and forecasting in the Urban Zone, Seattle, WA. American Meteorological Society, Boston

Athanassiadis GA, Rao ST, Clark RD (2002) Boundary layer evolution and its influence on ground-level ozone concentrations. Environ Fluid Mech 2:339–357

Balsley BB, Svensson G, Tjernstrom M (2008) On the scale-dependence of the gradient Richardson number in the residual layer. Boundary-Layer Meteorol 127:57–72

Banta RM, Mahrt L, Vickers D, Sun J, Balsley B, Pichugina Y, Williams E (2007) The very stable boundary layer on nights with weak low-level jets. J Atmos Sci 64:3068–3090

Banta RM, Pichugina YL, Brewer WA (2006) Turbulent velocity-variance profiles in the stable boundary layer generated by a nocturnal low-level jet. J Atmos Sci 63:2700–2719

Banta RM, Pichugina YL, Newsom RK (2003) Relationship between low-level jet properties and turbulence kinetic energy in the nocturnal stable boundary layer. J Atmos Sci 60:2549–2555

Banta RM, Senff CJ, White AB, Trainer M, McNider RT, Valente RJ, Mayor SD, Alvarez RJ, Hardesty RM, Parish DD, Fehsenfeld FC (1998) Daytime buildup and nighttime transport of urban ozone in the boundary layer during a stagnation episode. J Geophys Res D 103:22519–22544

Bloomer BJ, Vinnikov KY, Dickerson RR (2010) Changes in seasonal and diurnal cycles of ozone and temperature in the eastern U.S. Atmos Environ 44:1–9

Brown SS, Neuman JA, Ryerson TB, Trainer M, Dube WP, Holloway JS et al (2006) Nocturnal odd-oxygen budget and its implications for ozone loss in the lower troposphere. Geophys Res Lett 33:8

Chen F, Dudhia J (2001) Coupling an advanced land surface hydrology model with the Penn State-NCAR MM5 modeling system. Part I: model implementation and sensitivity. Mon Weather Rev 129:569–585

De Wekker SFJ, Berg LK, Allwine KJ, Doran JC, Shaw WJ (2004) Boundary-layer structure upwind and downwind of Oklahoma City during the Joint Urban 2003 field study. In: 5th symposium on the urban environment, Vancouver, BC. American Meteorological Society, Boston

Dudhia J (1989) Numerical study of convection observed during the winter monsoon experiment using a mesoscale twodimensional model. J Atmos Sci 46:3077–3107

Eliasson I, Thorsson S, Andersson-Skolfd Y (2003) Summer nocturnal ozone maxima in Goteborg, Sweden. Atmos Environ 37:2615–2627

Emmons LK et al (2010) Description and evaluation of the model for ozone and related chemical tracers, version 4 (MOZART-4). Geosci Model Dev 3:43–67

Environmental Protection Agency (EPA) (2010) Our Nation's air. Status and trends through 2008. EPA - 454/R-09-002, http://www.epa.gov/airtrends/2010/report/fullreport.pdf. Access 16 Jan 2011

Fitzjarrald DR, Moore KE (1994) Growing season boundary layer climate and surface exchanges in subarctic lichen woodland. J Geophys Res D 99:1899–1917

Geyer A, Stutz J (2004a) Vertical profiles of NO_3, N_2O_5, O_3, and NO_x in the nocturnal boundary layer: 2. Model studies on the altitude dependence of composition and chemistry. J Geophys Res 109. doi:10.1029/2003JD004211

Geyer A, Stutz J (2004b) The vertical structure of OH-HO_2-RO_2 chemistry in the nocturnal boundary layer: a one-dimensional model study. J Geophys Res D 109. doi:10.1029/2003JD004425

Gouveia FJ, Leach MJ, Shinn JH, Ralph WE (2007) Use of a large crane for wind and tracer profiles in an urban setting. J Atmos Oceanic Technol 24:1750–1756
Grimmond CSB, Su H-B, Offerle B, Crawford B, Scott S, Zhong S, Clements C (2004) Variability of sensible heat fluxes in a suburban area of Oklahoma City. In: Symposium on planning, nowcasting, and forecasting in the urban zone, Seattle, WA. American Meteorological Society, Boston
Guenther A, Zimmerman P, Wildermuth M (1994) Natural volatile organic compound emission rate estimates for U.S. woodland landscapes. Atmos Environ 28:1197–1210
Hidy GM (2000) Ozone process insights from field experiments part I: overview. Atmos Environ 34:2001–2022
Higgins RW, Yao Y, Yarosh ES, Janowiak JE, Mo KC (1997) Influence of the Great Plains low-level jet on summertime precipitation and moisture transport over the central United States. J Clim 10:481–507
Hong S-Y, Dudhia J, Chen S-H (2004) A revised approach to ice microphysical processes for the bulk parameterization of cloud and precipitation. Mon Weather Rev 132:103–120
Hong S-Y, Noh Y, Dudhia J (2006) A new vertical diffusion package with explicit treatment of entrainment processes. Mon Weather Rev 134:2318–2341
Hu X-M, Doughty DC, Sanchez KJ, Joseph E, Fuentes JD (2012) Ozone variability in the atmospheric boundary layer in Maryland and its implications for vertical transport model. Atmos Environ 46:354–364
Hu X-M, Klein P, Xue M, Zhang F, Doughty D, Forkel R, Joseph E, Fuentes JD (2013a) Impact of the vertical mixing induced by low-level jets on boundary layer ozone concentration. Atmos Environ 70:123–130
Hu X, Klein P, Xue M, Lundquist J, Zhang F, Qi Y (2013b) Impact of low-level Jets on the nocturnal urban heat island intensity in Oklahoma City. J Appl Meteorol Climatol. doi:10.1175/JAMC-D-12-0256.1
Hu X-M, Klein PM, Xue M, Shapiro A, Nallapareddy A (2013c) Enhanced vertical mixing associated with a nocturnal cold front passage and its impact on near-surface temperature and ozone concentration. J Geophys Res 118:2714–2728
Kastner-Klein P, Williams D, Hall F (2002) Impact of long-range transport on ozone pollution in the Oklahoma City metropolitan area. In: 12th joint conference on the applications of air pollution meteorology with the air and waste management association, May 20–24, Norfolk, VA, USA
Lundquist JK, Mirocha JD (2008) Interaction of nocturnal low-level jets with urban geometries as seen in joint urban 2003 data. J Appl Meteorol Climatol 47:44–58
McPherson RA, Fiebrich C, Crawford KC, Elliott RL, Kilby JR, Grimsley DL, Martinez JE, Basara JB, Illston BG, Morris DA, Kloesel KA, Stadler SJ, Melvin AD, Sutherland AJ, Shrivastava H (2007) Statewide monitoring of the mesoscale environment: a technical update on the Oklahoma Mesonet. J Atmos Oceanic Technol 24:301–321
Mlawer EJ, Taubman SJ, Brown PD, Iacono MJ, Clough SA (1997) Radiative transfer for inhomogeneous atmospheres: RRTM, a validated correlated-k model for the longwave. J Geophys Res 102D:16663–16682
Neu U, Kunzle T, Wanner H (1994) On the relation between ozone storage in the residual layer and daily variation in near-surface ozone concentration—a case study. Boundary-Layer Meteorol 69:221–247
Oke TR (1982) The energetic basis of the urban heat island. Q J R Meteorol Soc 108:1–24
Parish TR, Oolman LD (2010) On the role of sloping terrain in the forcing of the great plains low-level jet. J Atmos Sci 67:2690–2699
Philbrick CR, Ryan WF, Clark RD, Doddridge BG, Hopke PK, McDow SR (2003) Advances in understanding urban air pollution from the NARSTO-NEOPS program. In: 5th conference on atmospheric chemistry: gases, aerosols, and clouds, American Meteoroloical Society, 8–13 February 2003, Long Beach, CA
Pleim JE (2011) Comment on "Simulation of surface ozone pollution in the central Gulf coast region using WRF/Chem model: sensitivity to PBL and land surface physics". Adv Meteorol. doi:10.1155/2011/464753
Reitebuch O, Strassburger A, Emeis S, Kuttler W (2000) Nocturnal secondary ozone concentration maxima analysed by sodar observations and surface measurements. Atmos Environ 34:4315–4329
Samson PJ (1978) Nocturnal ozone maxima. Atmos Environ 12:951–955
Skamarock WC, Coauthors (2008) A description of the advanced research WRF version 3. NCAR technical note TN-475_STR, 113 pp
Solomon P, Cowling E, Hidy G, Furiness C (2000) Comparison of scientific findings from major ozone field studies in North America and Europe. Atmos Environ 34:1885–1920
Song J, Liao K, Coulter RL, Lesht BM (2005) Climatology of the low-level jet at the Southern Great Plains atmospheric boundary layer experiments site. J Appl Meteorol 44:1593–1606
Stockwell WR, Kirchner F, Kuhn M, Seefeld S (1997) A new mechanism for regional atmospheric chemistry modeling. J Geophys Res 102:25847–25879
Stutz J, Alicke B, Ackermann R, Geyer A, White A, Williams E (2004) Vertical profiles of NO_3, N_2O_5, O_3, and NO_x in the nocturnal boundary layer: 1. Observations during the Texas air quality study 2000. J Geophys Res 109. doi:10.1029/2003JD004209
Stutz J, Wong KW, Lawrence L, Ziemba L, Flynn JH, Rappenglück B, Lefer B (2009) Nocturnal NO_3 radical chemistry in Houston, TX. Atmos Environ. doi:10.1016/j.atmosenv.2009.03.004

Tong NYO, Leung DYC, Liu CH (2011) A review on ozone evolution and its relationship with boundary layer characteristics in urban environments. Water Air Soil Pollut. 214:13–36

Velasco E, Marquez C, Bueno E, Bernabe RM, Sanchez AO, Fentanes HW et al (2008) Vertical distribution of ozone and VOCs in the low boundary layer of Mexico City_acp-8-3061-2008. Atmos Chem Phys 8:3061–3079

Wexler H (1961) A boundary layer interpretation of the low-level jet. Tellus 13:368–378

Whiteman CD, Bian X, Zhong S (1997) Low-level jet climatology from enhanced rawinsonde observations at a site in the southern Great Plains. J Appl Meteorol 36:1363–1376

Zhang J, Rao ST (1999) The role of vertical mixing in the temporal evolution of ground-level ozone concentrations. J Appl Meteorol 38:1674–1691

Zhong S, Fast JD, Bian X (1996) A case study of the Great Plains low-level jet using wind profiler network data and a high-resolution mesoscale model. Mon Weather Rev 124:785–806